An observational study of the effects of aerosols on diurnal variation of heavy rainfall and the concurrent cloud changes over Beijing-Tianjin-Hebei

Siyuan Zhou[1,2,3], Jing Yang[1,2*], Wei-Chyung Wang[3], Chuanfeng Zhao[4], Daoyi Gong[1,2], Peijun Shi[1,2]

[1] State Key Laboratory of Earth Surface Process and Resource Ecology, Beijing Normal University, China

[2] Key Laboratory of Environmental Change and Natural Disaster, Faculty of Geographical Science, Beijing Normal University, China

[3]Atmospheric Sciences Research Center, State University of New York, Albany, New York 12203, USA

[4] College of Global Change and Earth System Science, Beijing Normal University, China

Submitted to ACP

Oct 2018

*Correspondence to: Jing Yang, State Key Laboratory of Earth Surface Process and Resource Ecology/ Key Laboratory of Environmental Change and Natural Disaster, Faculty of Geographical Science, Beijing Normal University, 19#Xinjiekouwai Street, Haidian District, Beijing 100875, China. E-mail: yangjing@bnu.edu.cn

Abstract: Our previous study found that the observed rainfall diurnal variation over Beijing-Tianjin-Hebei shows distinct signature of the effects of pollutants. Here we used the hourly rainfall data together with satellite-based daily information of aerosols and clouds to further investigate the effects of aerosols on heavy rainfall, and the concurrent changes of cloud properties. For heavy rainfall, three distinguished characteristics are identified: *earlier start time*, *earlier peak time*, and *longer duration*. The quantitative values of these changes are however sensitive to the choice of pollution indicators: 0.7, 1.0 and 0.8 hours based on aerosol optical depth (AOD); and 2.1, 4.2 and 2.4 hours based on cloud droplet number concentration (CDNC). In-depth analysis suggests that the characteristics of earlier in both start time and peak time occur in the presence of black carbon (absorbing aerosols) while the longer duration is attributed to sulfate (scattering aerosols) and increased low-level moisture (specific humidity at 850 hPa). Because of its close relevance to changes in heavy rainfall, we also examined changes of clouds. Significant increases in cloud fraction, cloud top pressure, the liquid/ice cloud optical thickness and cloud water path are exhibited. The liquid cloud effective radius is increased using AOD while the ice cloud effective radius is decreased using either AOD or CDNC. The moisture has the similar effect on cloud with the CDNC, which means that the aerosol effect may not be isolated from the impact of humidity. Finally, the mechanisms which may explain the aerosol effects are discussed and hypothesized.

Key words: aerosol, heavy rainfall, diurnal variation, cloud, Beijing-Tianjin-Hebei, observational study

1. Introduction

Aerosols modify the global hydrologic cycle through both radiative effect (direct effect) and cloud effect (indirect effect) (IPCC, 2013). On the one hand, through absorbing or scattering solar radiation, aerosols can lead to the air aloft heating (e.g. Jacobson 2001; Lau et al. 2006) or the surface cooling (Lelieveld and Heintzenberg 1992; Guo et al. 2013; Yang et al., 2018), which changes the atmospheric vertical static stability and modulates rainfall (e.g. Rosenfeld et al. 2008). On the other hand, water-soluble aerosols serving as cloud condensation nuclei (CCN) could affect the warm-rain processes and cold-rain processes through influencing the cloud droplet size distributions, cloud top heights and other cloud properties (Jiang et al., 2002; Givati and Rosenfeld 2004; Chen et al., 2011; Lim and Hong 2012; Tao et al., 2012). Beijing-Tianjin-Hebei (BTH) region is the heaviest aerosol polluted area in China and concerns have been raised about the aerosol-radiation-cloud-precipitation interaction over this region. The impact of aerosols on light rainfall or warm-rain processes over BTH region almost reaches consistent agreement (e.g., Qian et al., 2009), but aerosol effects on the heavy convective rainfall in this region still have large uncertainties (Guo et al., 2014; Wang et al., 2016).

The clouds that can generate heavy convective rainfall in BTH region usually contain warm clouds, cold clouds and mixed-phase clouds (e.g. Guo et al., 2015). Because the aerosol-cloud interactions in different

types of clouds are distinct (Gryspeerdt et al., 2014b), aerosol indirect effect during heavy rainfall is more complicated than its direct effect (Sassen et al., 1995; Sherwood, 2002; Jiang et al., 2008, Tao et al., 2012). For warm clouds, by serving as CCN that nucleates more cloud droplets, aerosols can increase cloud albedo so called albedo effect or Twomey effect (Twomey, 1977), lengthen the cloud lifetime so called lifetime effect (Albrecht, 1989), and enhance thin cloud thermal emissivity so called thermal emissivity effect (Garrett and Zhao, 2006). The above effects tend to increase the cloud microphysical stability and suppress warm-rain processes (Albrecht 1989; Rosenfeld et al. 2014). For cold clouds and mixed-phase clouds, many studies reported that the cloud liquid accumulated by aerosols is converted to ice hydrometeors above the freezing level, which invigorates deep convective clouds and intensifies heavy precipitation so called invigoration effect (Rosenfeld and Woodley, 2000; Rosenfeld et al., 2008; Lee et al. 2009; Guo et al. 2014). The Twomey effect infers that aerosols serving as CCN that increase the cloud droplets could reduce cloud droplet size within a constant liquid water path (Twomey, 1977). However, the opposite results of relationship between aerosols and cloud droplet effective radius were reported in observations (Yuan et al., 2008; Panicker et al., 2010; Jung et al., 2013; Harikishan et al., 2016; Qiu et al., 2017), which might be related with the moisture supply near the cloud base (Yuan et al., 2008; Qiu et al., 2017). Besides, the influence of aerosols on ice clouds also depends upon the amount of moisture supply (Jiang et al., 2008). Therefore, how the aerosols modify the heavy convective rainfall and concurrent cloud changes does not reach a consensus, particularly if considering the different moisture conditions.

Heavy convective rainfall over BTH region usually occurs within a few hours, thus studying on the relationship between aerosols and rainfall diurnal variation could deepen our understanding of aerosol effects on heavy rainfall. Several previous studies have found that aerosols are related to the changes of the rainfall diurnal variation in other regions (Kim et al., 2010; Gryspeerdt et al., 2014b; Fan et al., 2015; Guo et al., 2016; Lee et al., 2016). However, the above studies do not address the change of cloud properties and its sensitivity to different conditions of moisture supply. Although our recent work over BTH region (Zhou et al. 2018) attempted to remove the meteorological effect including circulation and moisture and found that the peak of heavy rainfall shifts earlier on the polluted condition, it only excluded the extreme moisture conditions and focused on aerosol radiative effect on the rainfall diurnal variation. Therefore, this study aims to deepen the previous study (Zhou et al., 2018) through investigating the following questions: (1) how do aerosols (including absorbing aerosols and scattering aerosols) modify the behaviors of the heavy rainfall diurnal variation (start time, peak time, duration and intensity)? (2) how do aerosols influence the concurrent cloud properties with inclusion of moisture? To solve above questions, we used aerosol optical depth (AOD) as a macro indicator of aerosol pollution and cloud droplet number concentration (CDNC) as a micro indicator of CCN served by aerosols respectively to compare the characteristics of heavy rainfall diurnal variation and the concurrent cloud properties between clean and polluted conditions, and applied aerosol index (AI) to distinguish the associated different effects of absorbing aerosols and scattering aerosols. In addition, we used the specific humidity (SH) at 850 hPa as an indicator of moisture supply condition to investigate the possible

effects of moisture on the rainfall and clouds and compared them with the effects of aerosols. The paper is organized as following: The data and methodology are introduced in Sect. 2. Section 3 addresses the relationship between aerosol pollution and diurnal variation of heavy rainfall, including the distinct characteristics of rainfall diurnal variation on clean/polluted conditions; the different behaviors of heavy rainfall diurnal variation along with the change of two different types of aerosols, and the comparison of heavy rainfall behaviors influenced respectively by moisture and aerosols. Section 4 describes the concurrent changes of cloud properties associated with pollution and examines the possible influences of CCN and moisture on the cloud properties. Section 5 makes a discussion on the distinct roles of aerosol radiative effect/cloud effect on the behaviors of heavy rainfall diurnal variation, as well as the uncertainties of different indicators and associated distinct results. Conclusion will be given in Sect. 6.

2. Data and methodology

2.1 Data

Four types of datasets from the year 2002 to 2012 (11 years) are used in this study, which include (1) precipitation, (2) aerosols, (3) clouds, and (4) other meteorological fields.

2.1.1 Precipitation data

To study the diurnal variation of heavy rainfall, the gauge-based hourly precipitation datasets are used, which were obtained from the National Meteorological Information Center (NMIC) of the China Meteorological Administration (CMA) (Yu et al., 2007) at 2420 stations in China from 1951 to 2012. The quality control made by CMA/NMIC includes the check for extreme values (the value exceeding the monthly maximum in daily precipitation was rejected), the internal consistency check (wiping off the erroneous records caused by incorrect units, reading, or coding) and spatial consistency check (comparing the time series of hourly precipitation with nearby stations) [Shen et al., 2010]. Here we chose 176 stations in the plain area of BTH region that are below the topography of 100 meter above sea level as shown in Fig.1, because we purposely removed the probable orographic influence on the rainfall diurnal variation, which is consistent with our previous work (Zhou et al., 2018). The record analyzed here is the period of 2002 to 2012.

2.1.2 Aerosol data

AOD is a proxy for the optical amount of aerosol particles in a column of the atmosphere and serves as one of indicators for the division of aerosol pollution condition in this study, which was obtained from MODIS (Moderate Resolution Imaging Spectroradiometer) Collection 6 L3 aerosol product with the horizontal resolution of 1°x1° onboard the Terra satellite (Tao et al., 2015). The quality assurance of marginal or higher confidence is used in this study. The reported uncertainty in MODIS AOD data is on the order of (-0.02-10%), (+0.04+10%) (Levy et al., 2013). The Terra satellite overpass time at the equator is around 10:30 local solar

time (LST) in the daytime, and the satellite data is almost missing when it is rainy during the overpass time. As shown in Fig.2, the occurrence of selected heavy rainfall events in this study is mainly later than the satellite overpass time. Therefore, the AOD used here represents the situation of the air quality in advance of heavy rainfall appearance.

The ultraviolet AI from Ozone Monitoring Instrument (OMI) on board the Aura satellite which was launched in July 2004, is used for detecting the different types of aerosols in this study. The OMI ultraviolet AI is a method of detecting absorbing aerosols from satellite measurements in the near-ultraviolet wavelength region (Torres et al., 1998). The positive values of ultraviolet AI are attributed to the absorbing aerosols such as smoke and dust while the negative values of AI stand for the non-absorbing aerosols (scattering aerosols) such as sulfate and sea salt (Tariq and Ali, 2015). The near-zero values of AI occur when clouds and Rayleigh scattering dominate (Hammer et al., 2018). The horizontal resolution of AI data is 1°×1° and it covers the period of 2005 to 2012.

MACC-II (Monitoring Atmospheric Composition and Climate Interim Implementation) reanalysis product produced by ECMWF (the European Centre for Medium-Range Weather Forecasts), provided the AOD datasets for different kinds of aerosols (BC, sulfate, organic matter, mineral dust and sea salt). MACC-II reanalysis products are observationally-based within a model framework, which can offer a more complete temporal and spatial coverage than observation and reduce the shortcomings of simulation that fail in simulating the complexity of real aerosol distributions (Benedetti *et al*., 2009). The horizontal resolution of MACC-II is also 1°×1° with the time interval of six-hour. MACC-II data covers the period of 2003 to 2012.

2.1.3 Cloud data

Daily cloud variables, including cloud fraction (CF), cloud top pressure (CTP), cloud optical thickness (COT, liquid and ice), cloud water path (CWP, liquid and ice) and cloud effective radius (CER, liquid and ice), were obtained from MODIS Collection 6 L3 cloud product onboard the Terra satellite. The MODIS cloud product combines infrared emission and solar reflectance techniques to determine both physical and radiative cloud properties (Platnick et al., 2017). The validation of cloud top properties in this product has been conducted through comparisons with CALIOP (Cloud-Aerosol Lidar with Orthogonal Polarization) data and other lidar observations (Holz et al., 2008; Menzel et al., 2008), and the validation and quality control of cloud optical products is performed primarily using in situ measurements obtained during field campaigns as well as the MODIS Airborne Simulator instrument (https://modis-atmos.gsfc.nasa.gov/products/cloud). Consistent with AOD, the measure of above cloud variables is before the occurrence of heavy rainfall.

CDNC is retrieved as the proxy for CCN and also another indicator for separating different aerosol conditions in this study. Currently, most derivations of CDNC assume that the clouds are adiabatic and horizontally homogeneous; CDNC is constant throughout the cloud's vertical extent, and cloud liquid water

content varies linearly with altitude adiabatically (Min et al., 2012; Bennartz and Rausch, 2017). According to Boers et al. (2006) and Bennartz (2007), we calculated CDNC (unit: cm^{-3}) through:

$$\mathrm{CDNC} = \frac{{C_W}^{1/2}}{k} \frac{10^{1/2}}{4\pi {\rho_w}^{1/2}} \frac{\tau^{1/2}}{{R_e}^{5/2}} \quad (1)$$

Where C_w is the moist adiabatic condensate coefficient, and its value depends slightly on the temperature of the cloud layer, ranging from 1 to 2. 5 x 10^{-3} gm^{-4} for a temperature between 0 ℃ and 40 ℃ (Brenguier, 1991). In this study, we calculated the C_w through the function of the temperature (see Fig.1 in Zhu et al., 2018) at a given pressure that is 850 hPa. And we have tested the sensitivity of CDNC to the amount of C_w and found it almost keeps the same when the C_w changes from 1 to 2. 5 x 10^{-3} gm^{-4}. The coefficient k is the ratio between the volume mean radius and the effective radius and varies between 0.5 and 1 (Brenguier et al., 2000). Here we used k = 1 for that we cannot get the accurate value of k and the value of k does not influence the rank of CDNC for the division of aerosol condition in this study. ρ_w is cloud water density. τ and Re are the liquid COT and CER obtained from MODIS Collection 6 L3 cloud product onboard the Terra satellite with resolution of 1°x1°. To reduce the uncertainty of CDNC retrieval caused by the heterogeneity effect from thin clouds (Nakajima and King, 1990; Quaas et al., 2008; Grandey and Stier, 2010; Grosvenor et al., 2018), we selected the CF more than 80%, the liquid COT more than 4 and the liquid CER more than 4 μm when calculating the CDNC (Quaas et al., 2008).

2.1.4 Other meteorological data

Other meteorological factors, including wind, temperature, pressure and SH, were obtained from the ERA-Interim reanalysis datasets with 1°x1°horizontal resolution and 37 vertical levels at six-hour intervals. ERA-Interim is a global atmospheric reanalysis produced by ECMWF, which covers the period from 1979 to near-real time (Dee et al., 2011). The SH, which stands for the water vapor content, serves as the indicator of moisture supply condition in this study.

2.2 Methodology

2.2.1 Method of interpolation

We used both station data of gauge-based precipitation and gridded data including aerosols, clouds and other meteorological variables. Gridded datasets in this study were downloaded with the horizontal resolution of 1°×1°, which are consistent with the resolution of MODIS L3 product. To unify the datasets, we interpolated all the gridded datasets onto the selected 176 rainfall stations using the average value in a 1°×1° grid as the background condition of each rainfall station, i.e., the stations in the same 1°×1° grid have the same aerosol, cloud and meteorological conditions.

2.2.2 Selection of sub-season and circulation

Consistent with our previous work, we focused on early summer (1 June to 20 July) before the large-scale rainy season starts, in order to remove the large-scale circulation influence and identify the effect of aerosols on local convective precipitation because BTH rainfall during this period is mostly convective rainfall (Yu et al., 2007) with heavy pollution (Zhou et al., 2018). And to unify the background atmospheric circulation, we only selected the rainfall days with southwesterly flow, which is the dominant circulation accounting for 40% of total circulation patterns over the BTH region during early summer (Zhou et al., 2018).

2.2.3 Classification of the heavy rainfall, clean/polluted and moisture conditions

With the circulation of southwesterly, we selected heavy rainfall days when the hourly precipitation amount is more than 8.0 mm/hour (defined by *Atmospheric Sciences Thesaurus, 1994*). Here "a day" is counted from 8 LST to 8 LST next day (0 UTC to 24 UTC). We used two indicators to distinguish the clean and polluted conditions, which are AOD and CDNC. The 25^{th} and 75^{th} percentiles of AOD/CDNC of the whole rainfall days are used as the thresholds of clean and pollution condition, and the values are shown in Tab.1. It shows that there are 514 cases of heavy rainfall on polluted days and 406 cases of that on clean days when using AOD, and 630/716 cases on polluted/clean condition when using CDNC.

The absorbing aerosols are detected using the positive values of AI that is named as absorbing aerosol index (AAI) here, and we can retrieve the scattering aerosol index (SAI) using the negative values of AI. AAI and SAI are also divided into two groups using the threshold of 25^{th}/75^{th} percentile as shown in Tab.1. We used AAI/SAI more than 75^{th} as the extreme circumstances of absorbing/scattering aerosols to compare their impacts on heavy rainfall. The case numbers are 375 and 550 respectively for the extreme AAI and SAI cases. Using the same method, we chose cases with more BC/sulfate when the AOD of BC/sulfate is larger than the 75^{th} percentile of itself in all rainy days, and cases with less BC/sulfate when that is less than the 25^{th} percentile of itself in the same situation. Accordingly, we selected 459 heavy rainfall cases with more BC and 274 cases with less BC. Similarly, 361 cases with more sulfate and 419 cases with less sulfate with heavy rainfall were selected.

The SH at 850 hPa is used as the indicator of moisture supply under the cloud base. We chose wet cases when the SH on that day is larger than 75^{th} percentile of the whole rainy days, and chose dry cases when SH on that day is less than the 25^{th} percentile of the whole rainy days (the thresholds are shown in Tab. 1).

2.2.4 Statistical analysis

We adopted the probability distribution function (PDF) to compare the features of heavy rainfall and cloud variables on different conditions of aerosols, through which we can understand the changes of rainfall/cloud properties more comprehensively. The numbers of bins we selected in the study have been all tested for better representing the PDF distribution. Student's t-test is used to examine the significance level of differences between the different groups of aerosol conditions.

3. Relationship between aerosol pollution and diurnal variation of heavy rainfall over BTH

3.1 Distinct characteristics of heavy rainfall diurnal variation associated with aerosol pollution

Our previous study (Zhou et al. 2018) has reported the distinct peak shifts of rainfall diurnal variation between clean and polluted days using the indicator of AOD over the BTH region during early summer. Similar with our previous study, the PDF of the heavy rainfall peak time shows that the maximum of rainfall peak is about two hours earlier on the polluted days (20:00 LST) than that on the clean days (22:00 LST) (Fig. 2a). To comprehensively recognize the changes of rainfall diurnal variation associated with air qualities, here we examined the PDF of the start time, the duration and the intensity besides the peak time of heavy rainfall.

As shown in Fig. 2a, the start time of heavy rainfall exhibits a significant advance on the polluted days. The secondary peak on the early morning is ignored here because the early-morning rainfall is usually associated with the mountain winds (Wolyn et al., 1994; Li et al., 2016) and the nighttime low-level jet (Higgins et al., 1997; Liu et al., 2012) that is beyond the scope of this study. The time for the maximum frequency of heavy rainfall initiation is around 6 hours earlier on the polluted days, shifting from around 0:00 LST on the clean days to the 18:00 LST (Fig. 2a). Regarding the rainfall durations, the average persistence of heavy rainfall on polluted days is 0.8 hours longer than that on clean days (Tab. 2). According to the PDF shown as in Fig. 2a, the occurrence of short-term precipitation (≤6 hours, Yuan et al., 2010) decreases while that of long-term precipitation (>6 hours, Yuan et al., 2010) increases. The intensity of hourly rainfall exhibits a non-significant increase on the polluted days.

The distinct behaviors of heavy rainfall diurnal variation between clean and polluted days have been well demonstrated using the indicator of AOD. However, AOD is not a proper proxy for CCN (Shinozuka et al., 2015) but the property of aerosols serving as CCN should be considered because aerosol-cloud interaction plays an indispensable role on changing rainfall diurnal variation. Therefore, here we applied the retrieved CDNC as the indicator of CCN (Zeng et al., 2014; Zhu et al., 2018) to examine the above-mentioned results. As a result, the similar changes of heavy rainfall can be well exhibited in CDNC analysis as shown in Fig. 2b. The start time and peak time of heavy rainfall on the polluted condition also show significant advances compared with that on the clean condition, with the average advances of 1.4 hours and 3.0 hours respectively (Tab. 2). The duration of heavy rainfall on the polluted condition is also prolonged, which is 2.2 hours longer in average (Tab. 2). Similar with the results based on AOD, the difference of rainfall intensity between clean and polluted conditions using CDNC does not pass the 95% statistical confidence level as well.

Hence, the results using either AOD or CDNC show that the start and peak time of heavy rainfall occur earlier and the duration becomes longer under pollution, although there are some quantitative differences between the two indicators. Since the difference of rainfall intensity is not significant in this study, the following analysis only focuses on studying the start time, peak time and duration of heavy rainfall along with aerosol pollution.

3.2 Distinct behaviors of heavy rainfall diurnal variation associated with two different types of aerosols

Using the indicator of AI, we further investigated the distinct behaviors of heavy rainfall diurnal variation related to absorbing aerosols and scattering aerosols respectively. The PDF of start time, peak time and duration of heavy rainfall under the extreme circumstances of absorbing aerosols and scattering aerosols are compared in Fig. 3. Here, we briefly named the days with extreme large amount of absorbing aerosols as absorbing aerosol days and with more scattering aerosols as scattering aerosol days. The start time of heavy rainfall on absorbing aerosol days shows a significant earlier compared with that on scattering aerosol days (Fig. 3a), with 0.7 hours advance in average (Tab. 3). Similarly, the rainfall peak time also shows earlier on absorbing aerosol days (Fig. 3b), with an average advance of 1.6 hours (Tab. 3). The rainfall duration on scattering aerosol days shows longer than that on absorbing aerosol days, which are 6.0 hours and 5.0 hours respectively in average (Tab. 3). All the above-mentioned differences between the two groups have passed 95% statistical confidence level. The results indicate that the absorbing aerosols and scattering aerosols may have different or inverse effects on the heavy rainfall that absorbing aerosols may generate the heavy rainfall in advance while the scattering aerosols may delay and prolong the heavy rainfall.

To further verify the different behaviors of heavy rainfall diurnal variation associated with two different types of aerosols, we purposely re-examine the above-mentioned phenomena using BC/sulfate that can represent typical absorbing/scattering aerosols over the BTH region. BC has its maximum center over BTH region (Fig. 4a) and our previous study has indicated that the radiative effect of BC low-level warming may facilitate the convective rainfall generation (Zhou et al., 2018). The percentage of sulfate is also large over the BTH region (Fig. 4b) and the sulfate is one of the most effective CCN that influences the precipitation in this region (Gunthe et al., 2011). Accordingly, we selected the cases with different amounts of BC and sulfate AOD to compare their roles on the diurnal variation of heavy rainfall. The methods have been described in Sect. 2.2.3. The PDF of the start time, peak time and duration of heavy rainfall in the cases with more/less amount of BC are shown in Fig. 5a, respectively. The most striking result is that the maximum frequency of rainfall start time in the more BC cases evidently shifts earlier (Fig. 5a). Meanwhile, the mean peak time in the more BC cases shows 1.1 hour earlier than that in the less BC cases (Tab. 3). And the duration of heavy rainfall is slightly shortened by the averaged 0.2 hours in the more BC cases. The features in more BC cases are consistent with the above results of absorbing aerosols. In contrast, when the sulfate has higher amount, the mean start time of rainfall is delayed by 0.5 hours, while the duration shows a significant increase by 1.5 hours in average (Tab. 3). The behaviors in the more sulfate cases also exhibit similar with the above results of scattering aerosols, except for the peak time that shows later in the scattering aerosol cases but a little earlier in the more sulfate cases (Tab. 3).

306 **3.3 Behavior comparisons of heavy rainfall diurnal variation influenced by moisture and aerosol.**

307 Moisture supply is an indispensable factor for the precipitation formation. Since the southwesterly circulation
308 can not only transport pollutants but also plenty of moisture to the BTH region (Wu et al., 2017), more
309 pollution usually corresponds to more moisture for the BTH region (Sun et al., 2015) so that it is hard to
310 completely remove the moisture effect on the above results in the pure observational study. Here we attempt
311 to recognize the moisture effect on the heavy rainfall to further understand the above aerosol-associated
312 changes. Because the moisture supply for BTH is mainly transported via low-level southwesterly circulation,
313 we purposely used the SH at 850 hPa as the indicator of moisture condition.

314 Using the similar percentile method with polluted/clean days, we got the rainfall characteristics in the more
315 humid (more than 75th percentile) and the less humid (less than 25th percentile) environments on the heavy
316 rainfall days regardless of the aerosol condition, as shown in Fig. 6a. The results show that the start time of
317 heavy rainfall is delayed by 0.9 hours, the peak time is 0.6 hours earlier and the duration is prolonged by 2.0
318 hours in average in the more humid environment, which is similar with the results of the more sulfate cases.
319 Besides, the same results are obtained with different moisture indicator, e.g. the 850 hPa absolute humidity.
320 These results indicate the advance of heavy rainfall start time on the polluted days is not caused by more
321 moisture supply, while the longer duration and earlier peak in the more sulfate cases might be related to the
322 increased moisture supply.

323 We also investigate the distributions of moisture and rainfall behaviors in the clean and polluted cases
324 respectively using AOD and CDNC (Fig. 6 b&c). The results show that the relationship between moisture and
325 rainfall start time/peak time/duration is not linear. Using either AOD or CDNC, the distribution of SH exhibits
326 a slight increase in the polluted cases, indicating that the polluted cases have the more moisture than the clean
327 cases which is particularly well shown using AOD. However, when fixing the moisture at a certain range
328 especially at the relative dry condition, we can detect the similar phenomena of earlier start/peak time and
329 longer duration in the polluted cases. For example, when the amount of 850 hPa SH is between 8-12 g/kg, the
330 start &peak time in the polluted cases show significant earlier and the duration exhibits slightly increased
331 compared with that in the clean cases using either AOD or CDNC.

332 The above results indicate that the advance of heavy rainfall start and peak time in the polluted cases might
333 be weakly related to the moisture effect, but the moisture could obviously prolong the duration of heavy
334 rainfall (Fig. 6a). Because the diurnal change of heavy rainfall with more moisture is similar with the
335 behaviors of heavy rainfall with scattering aerosols especially sulfate, we cannot figure out their individual
336 role at present.

337

338 **4 Relationship between aerosol pollution and concurrent changes of cloud properties associated with**
339 **heavy rainfall diurnal variation**

4.1 Concurrent changes of cloud properties along with heavy rainfall diurnal variation on clean and polluted conditions

To understand the cloud effect of aerosols during heavy rainfall diurnal variation, we need to recognize the concurrent cloud characteristics on the clean and polluted conditions. The cloud properties we used were obtained from satellite product that were measured at the same time with aerosols before the occurrence of heavy rainfall. The differences of cloud features were examined in both macroscopic (including CF, CTP, COT and CWP) and microscopic properties (including CER) between the clean and polluted conditions based on AOD and CDNC respectively, as shown in Fig. 7.

Using AOD as the pollution indicator, the PDF distribution of CF shows that the CF on the polluted condition is evidently larger than that on the clean condition. The average CF is 62.8% on the clean condition, and 89.3% on the polluted condition (Tab. 4), which is increased by 26.1%. The average CTP on the polluted condition is 487.3 hPa, which is larger than 442.3 hPa on the clean condition and increases 45 hPa, indicating that the cloud top height is lower on the polluted days. The COT, CWP and CER were further analyzed for the liquid and ice portions of clouds as shown in Fig. 7. Both liquid and ice COT on polluted condition exhibit significant increases compared with that on clean condition. The mean amount of liquid COT is increased by 3.1 and ice COT increases by 6.2 (Tab. 4). Similar with COT, the amount of liquid and ice CWP also increase on polluted condition, which increase by 33.6 g/m^2 and 88.2 g/m^2 respectively. In addition, the liquid CER is increased by 0.8 μm and the ice CER is decreased by 2.8 μm on the polluted days. The differences of above cloud properties between clean and polluted cases have all passed the 95% statistical confidence level.

Using CDNC as another pollution indicator, the above-mentioned changes of cloud properties are consistent with that using AOD, except for liquid CER (Fig. 7). Since the calculation method of CDNC is not independent on the liquid COT and liquid CER, we would not directly compare the results of liquid COT and CER based on CDNC with those based on AOD here. But according to other variables that are independent of the CDNC calculation, we found the cases with more CDNC are accompanied with the increase of CTP, ice COT and liquid & ice CWP, which increase by 32.8 hPa, 24.4, 215.8 g/m^2 and 370.9 g/m^2 respectively (Tab 4) and all of which are consistent with the results based on AOD. The CER of ice clouds also shows a consistent decrease by 8.8 μm on the polluted condition based on CDNC. We noticed that the changes of the COT/CWP/CER for both liquid and ice based on CDNC are much larger than that based on AOD, which indicates that these cloud properties might be more sensitive to the indicator of CDNC rather than AOD.

According to the above comparison, the concurrent changes of cloud properties along with heavy rainfall diurnal variation show consistent results using the two pollution indicators (AOD and CDNC). The pollution corresponds to the increase of CF, ice COT, liquid and ice CWP, but the decrease of cloud top height (the increase of CTP corresponds to the decrease of cloud top height) and ice CER. With the increase of AOD, both the liquid COT and liquid CER are increased. Since we cannot distinguish the liquid part of mix-phased clouds from liquid (warm) clouds in the observation, the changes of liquid cloud properties above might come

from both the liquid (warm) clouds and the liquid part of mixed-phase clouds. Likewise, the above-mentioned changes of ice cloud properties might come from both ice (cold) clouds and the ice part of mixed-phase clouds.

4.2 Influences of CDNC (CCN) and moisture on the cloud properties

Section 3.3 has shown that the diurnal variation of heavy rainfall with more moisture supply is similar with the changes of heavy rainfall with more sulfate aerosol. We assume that the moisture under the cloud base and the sulfate serving as CCN both influence the cloud properties (Yuan et al., 2008; Jiang et al., 2008; Jung et al., 2013; Qiu et al., 2017). To identify the effect of aerosols on clouds and its sensitivity to moisture, we purposely investigated the changes of above cloud properties with different conditions of the CDNC and the low-level moisture (850hPa SH) respectively. We categorized all cases of heavy rainfall into four groups, which are (1) clean and dry, (2) polluted and dry, (3) clean and wet, (4) polluted and wet, and checked the changes of above cloud properties, as shown in Tab. 5. To retrieve the comparable samples, here "clean/polluted" refers to the CDNC on that rainfall day less/more than $25^{th}/75^{th}$ percentile of the CDNC among the heavy rainfall days, and similarly, the "dry/wet" refers to the SH on that rainfall day less/more than $25^{th}/75^{th}$ percentile of itself among the heavy rainfall days. The average CDNC is 68.58 cm^{-3} on the dry condition and 68.56 cm^{-3} on the wet condition, and the average SH is 11.3 g/kg and 11.8 g/kg on the clean and polluted conditions respectively, thus we can consider the CDNC or SH remain the same when the other condition changes. We made the significant test of differences between group 1 and 2, group 1 and 3, group 2 and 4, group 3 and 4. Because the CF is fixed above 80% when calculating the CDNC (see in Sect. 2.1.3), here the selected groups all belong to the condition of higher CF.

Comparing the results of group 1 and 2, which are both on the dry condition, we can identify the influence of CDNC on the cloud properties, which stands for the effect of CCN. The changes of these cloud variables are the same as that in Sect. 4.1, that the CF, ice COT and liquid & ice CWP are increased on the polluted condition, while the cloud top height and ice CER are decreased based on CDNC. Among these variables, the ice COT and liquid & ice CWP are especially larger on the polluted condition, which are 5-6 times larger than that on the clean condition (Tab. 5). On the wet condition, comparing the group 3 and 4, the changes are similar that the CF, ice COT and liquid & ice CWP are increased and the ice CER are decreased but the change of CTP becomes not significant. However, the changes of these variables on the dry condition are evidently enhanced than that on the wet condition, which indicates these cloud properties might be more sensitive to CDNC on the dry condition. The above comparisons indicate that with the increase of CDNC (CCN), the CF, ice COT and liquid & ice CWP are increased while the ice CER is decreased regardless of the moisture amount. Although the comparisons of liquid COT and liquid CER based on CDNC are meaningless since the CDNC is calculated by the two variables, we infer that the increase of liquid COT and the decrease of liquid CER (Tab. 5) might be not completely caused by CDNC calculation but the natural effect of CCN.

Comparing the results of group 1 and 3, we can get the changes of cloud properties related only to moisture on the same clean condition. A common feature is that CTP, COT and CWP both for liquid and ice exhibit increases along with the increase of moisture. Compared with the CTP on the clean and dry condition, it increases on both polluted & dry condition (group 2) and clean & wet condition (group 3), but on the former condition its increase is larger, which indicates the influence of moisture on CTP might be secondary compared to the CDNC (CCN) effect. Similarly, comparing the COT/CWP in group 2 and 3, the increases of COT and CWP both for liquid and ice in group 2 are 3-6 times larger than that in group 3, which indicates that the influences of moisture on COT and CWP may not overcome the influence of CCN. With the increase of moisture, the change of liquid CER is not significant on the same clean condition, but the ice CER is significantly decreased. On the polluted condition, comparing group 2 and 4, we found the COT and CWP both for liquid and ice on the wet condition are evidently smaller than that on the dry condition, which indicates that increasing the moisture might partly compensate for the influence of CDNC (CCN) on COT/CWP.

The results above indicate that both CDNC (CCN) and moisture have impacts on cloud properties. They both contribute to the increase of CF, COT and CWP, in which the influence of CDNC (CCN) on COT and CWP are significantly larger than moisture. The increase of either CDNC or moisture corresponds to the increase of CTP. But when the CDNC and moisture increase simultaneously, the CTP becomes smaller. Both CDNC and moisture correspond to the significant decrease of ice CER, while only CDNC corresponds to the decrease of liquid CER and that might be ascribed to the calculation method of CDNC. To reduce uncertainties, we have tested the SH at different levels (e.g., 700 hPa and 800 hPa) and different moisture indicator (e.g. absolute humidity) to verify above results, and found most cloud variables show the similar changes with the above except for the CTP and the liquid CER, which indicates the changes of CTP and liquid CER are more sensitive and have larger uncertainties. Since the behaviors of cloud changes are similar along with the increase of either CDNC (CCN) or moisture but more sensitive to the former, the results in Sect. 4.1 might actually reflect the combined effect of CCN and moisture, and the aerosol effect on these cloud properties might be dominant on the polluted days.

5. Discussion

5.1 Different roles of aerosol radiative effect and cloud effect in heavy rainfall

In Sect. 3 we found that the heavy rainfall has earlier start and peak time, and longer duration on the polluted condition. And afterwards, the earlier start of rainfall under pollution was found related to absorbing aerosols mainly referring to BC (Fig. 3a&5a). We also compared the effect of BC on the associated clouds. Figure 8a shows the CF larger than 90% rarely occurs in the more BC environment, which might be associated with the semi-direct effect of BC (Ackerman, 2000) or estimated inversion strength and BC

co-vary. This result indicates the influence of BC on the heavy rainfall in Fig. 5a is mainly due to the radiative effect rather than the cloud effect. The mechanism of BC effect on the heavy rainfall can be interpreted by our previous study (Zhou et al., 2018) as: BC absorbs shortwave radiation during the daytime and warms the lower troposphere at around 850 hPa, and then increases the instability of the lower to middle atmosphere (850-500hPa) so that enhances the local upward motion and moisture convergence. As a result, the BC-induced thermodynamic instability of the atmosphere triggers the occurrence of heavy rainfall in advance. Thus, the low-level heating effect of BC might play a dominant role in the beginning of rainfall especially before the formation of clouds during the daytime.

The delayed start of heavy rainfall with scattering aerosols in Fig. 3a and more sulfate in Fig. 5b is consistent with many studies that both the radiative effect and cloud effect of sulfate-like aerosols could delay or suppress the occurrence of rainfall (Guo et al., 2013; Wang et al., 2016; Rosenfeld et al. 2014). Sulfate-like aerosols as scattering aerosols could prevent the shortwave radiation from arriving at the surface thus cool the surface and stabilize the atmosphere, which suppresses the rainfall formation (Guo et al., 2013; Wang et al., 2016). Sulfate-like aerosols serving as CCN can also suppress the rainfall by cloud effect through reducing the cloud droplet size and thus suppressing the collision-coalescence process of cloud droplets (Albrecht 1989; Rosenfeld et al. 2014). Figure 8b does shows that in contrast with BC, the CF larger than 90% is significantly increased in the more sulfate environment, which indicates the sulfate-like aerosols might have more evident influence on the clouds and subsequently the rainfall changes associated with sulfate are probably due to the cloud effects. Another significant feature is the longer duration of heavy rainfall in both the scattering aerosol cases and more sulfate cases (Fig 3c&5b). Since the heavy rainfall shows the similar changes of delayed start and longer duration with the increase of sulfate and moisture, we currently cannot separate their respective roles in this study. We speculate that the postponed start of heavy rainfall is mainly due to the effect of sulfate-like aerosols. While the longer duration is caused by both the cloud effect of sulfate-like aerosols and the increased moisture supply, because increasing either CCN or the moisture supply can increase cloud water (Sect. 4.2), which could lead to the longer rainfall duration. To further investigate the mechanism of longer duration, we need the assistance of numerical model simulations in the future work.

Accordingly, we speculate that the earlier start time of heavy rainfall related to absorbing aerosols (BC) is due to the radiative heating of absorbing aerosols, while the longer rainfall duration is probably caused by both the cloud effect of sulfate-like aerosols and the increased moisture supply. As a summary we use a schematic diagram (Fig. 9) to illustrate how aerosols modify the heavy rainfall over the BTH region. On one hand, BC heats the lower troposphere, changing the thermodynamic condition of atmosphere, which increases upward motion and accelerates the formation of cloud and rainfall. On the other hand, the increased upward motion transports more sulfate-like particles and moisture into the clouds so that more CCN and sufficient moisture increase the cloud water, thus might prolong the duration of rainfall. As a result, the heavy rainfall over BTH region in southwesterly shows earlier start and peak time, and longer duration might due to the combined effect of aerosol radiative effect, aerosol cloud effect as well as moisture effect. To further

distinguish the individual effect, we need to conduct numerical model simulations in our future study.

5.2 Uncertainties of different indicators and associated distinct results

The gauge-based hourly precipitation data used in this study is more reliable than other observational and reanalysis precipitation data. In contrast with precipitation datasets, the observation of aerosols and clouds from MODIS might have larger uncertainties, e.g., which come from the misdetection of CF when AOD is large (Brennan et al., 2005; Levy et al., 2013) or the mutual interference between liquid and ice clouds (Holz et al., 2008; Platnick et al., 2017).

In this study we used two pollution indicators, AOD and CDNC, which discriminates the pollution levels for different purposes. AOD is a good proxy for the large-scale pollution level, but it stands for the optical feature of aerosols and cannot well represent CCN when we studied the aerosol-cloud interaction (Shinozuka et al., 2015). The value of AOD is also influenced by moisture condition, which is aerosol humidification effect (Twohy et al., 2009; Altaratz et al., 2013). Therefore, we comprehensively analyzed the moisture effect on the results. CDNC is a better proxy for CCN, which facilitates the study on the cloud changes associated with aerosol pollution. But the retrieved CDNC has larger uncertainties. First, the assumptions in the calculation of CDNC are idealized that CDNC is constant with height in a cloud and cloud liquid water increases monotonically at an adiabatic environment (Grosvenor et al., 2018), but the target of this study is the convective clouds with rainfall that may be not consistent with the adiabatic assumption. Second, as indicated by Grosvenor et al. (2018), the uncertainties in the pixel-level retrievals of CDNC from MODIS with 1°x1° spatial resolution can be above 54%, which come from the uncertainties of parameters and the original COT and CER data using in the calculation, and also the influence of heterogeneity effect from thin clouds. To reduce the influence of heterogeneity effect as much as possible, we have attempted to limit the conditions of CF, liquid COT and CER when calculating CDNC in the study. Besides, this study primarily focuses on the relative changes of CDNC, which may be also influenced by the potential systematic biases in the CDNC calculation, but actually reduced the uncertainties of absolute values.

We applied ultraviolet AI and AOD of BC/sulfate to identify different types of aerosols. The AI datasets from OMI, which can distinguish the absorbing aerosols and scattering aerosols, also have uncertainties especially for the near-zero values. Hence, we only compare the extreme circumstances of absorbing aerosols and scattering aerosols. We also found the AI has a weak positive correlation with AOD from MODIS, which indicates the results on absorbing aerosol days might represent the results on polluted days if identified by AOD. To avoid the uncertainty, we re-examined the results using AI when removing the polluted cases identified by AOD, and found the major results are not changed. The comparisons of BC/sulfate AOD cases also have uncertainties because they are retrieved from MACC reanalysis data. Although the above four indicators have their own uncertainties, currently we cannot find more reliable datasets in a long-term

observational record. The major findings using these four indices could well identify the changes of rainfall and clouds accompanied with aerosols, but are insufficient to clarify the aerosol effect on clouds and precipitation.

Using AOD and CDNC we have drawn the same conclusion that the heavy rainfall occurs in advance and the duration is prolonged under pollution (Fig. 2). We found the AOD and CDNC only have a weak positive correlation, which denotes that the selected cases could be different between using AOD and CDNC. The cases of heavy rainfall using CDNC seem more extreme, because CDNC cases exhibit more evident changes of rainfall behaviors in average than that using AOD. The quantitative difference of results between the two indicators might due to the non-linear relationship of CCN and pollution that the CCN won't continuously increase when aerosol loading is huge (e.g., Jiang et al., 2016), or due to the misdetection of AOD, the calculation uncertainty of CDNC, and the sampling differences between AOD and CDNC. Since both the two indicators have their uncertainties, we cannot say the result of which one is more reliable.

Most cloud properties also exhibit the consistent changes using AOD and CDNC. First, the CF and CWP (liquid and ice) increase with pollution, might because the aerosols serving as CCN can nucleate a larger number of cloud droplets and accumulate more liquid water in the cloud thus increase the CF and CWP. Second, the CTP increases under pollution using both AOD and CDNC, which denotes the decrease of the cloud top height. We speculate that the earlier start of the precipitation process could inhibit the vertical growth of clouds shown as in Fig. 2. Third, the ice CER decreases under pollution using either AOD or CDNC, which could be ascribed to that the increased cloud droplet number leads to more cloud droplets transforming into ice crystals and causes the decrease of ice CER (Chylek et al., 2006; Zhao et al., 2018; Gryspeerdt et al., 2018). Currently the detailed physical processes of cold clouds and mixed-phase clouds are not clear, including the diffusional grow, accretion, riming and melting process of ice precipitation (Cheng et al., 2010), which needs numerical model simulations to be further explored.

However, the results of liquid CER might have more uncertainties. The liquid CER is increased when AOD increases (Fig. 7), which might be related to the aerosol humidification effect, the misdetection of AOD and cloud water, and also might result from the earlier formation of the clouds and heavy rainfall on the polluted days. In addition, the relationships between satellite AOD and some cloud properties have been shown to be affected by meteorological co-variations, e.g., high humid could lead to strong positive relationship of AOD and CF (Quaas et al., 2010; Grandey et al., 2013) and the relationship of AOD and CTP could be also affected by meteorology (Gryspeerdt et al., 2014a), which indicates that the changes of cloud properties in this study might be influenced by the meteorological co-variations rather than the aerosol effect. Although we have considered the influence of moisture on the precipitation and clouds, the moisture variables cannot completely represent all the meteorological co-variations between aerosol and precipitation (Boucher and Quaas, 2012).

6. Conclusions

Using the gauge-based hourly rainfall records, aerosol and cloud satellite products and high temporal resolution reanalysis datasets during 2002-2012, this study investigated the different characteristics of heavy rainfall in the diurnal time scale on the clean and polluted conditions respectively. Based on two indicators that are AOD from MODIS aerosol product and retrieved CDNC from MODIS cloud product, we found three features of heavy rainfall changing by aerosols that the rainfall start and peak time occur earlier and the duration becomes longer. The quantitative differences exist between the two indicators, i.e., the statistic differences of above features between clean and polluted conditions are 0.7, 1.0, 0.8 hours based on AOD and 1.4, 3.0, 2.2 hours based on CDNC. The different relationships of absorbing and scattering aerosols to the diurnal shift were also distinguishable using ultraviolet AI from OMI and reanalysis AOD of two aerosol types (BC and sulfate). The absorbing aerosols (BC) correspond to the earlier start time and peak time of heavy rainfall, while the scattering aerosols (sulfate) correspond to the delayed start time and the longer duration. To distinguish the influence of aerosols, the influence of moisture (SH at 850 hPa) on the heavy rainfall is also investigated, which shows similar with the scattering aerosols (sulfate), that means the aerosol effect may not be isolated from the impact of humidity. By comparing the characteristics of cloud macrophysics and microphysics variables, using both AOD and CDNC we found the CF, ice COT, liquid and ice CWP are increased on the polluted condition, but the cloud top height and the ice CER are reduced. Liquid COT and liquid CER are also increased in AOD analysis. Comparing the influence of CDNC (which represents CCN) and moisture respectively on these cloud variables, the cloud properties show similar changes with the increase of CDNC and moisture, but seem more sensitive to the CDNC (CCN).

According to these results, we speculate that both aerosol radiative effect and cloud effect have impacts on the diurnal variation of heavy rainfall in the BTH region. The heating effect of absorbing aerosols especially BC increases the instability of the lower to middle atmosphere so that generates the heavy rainfall occurrence in advance. And the increased moisture supply and increased aerosols which nucleate more cloud droplets and accumulate more liquid water in clouds, leading to the longer duration of heavy rainfall.

This study has clearly identified the relationship of the aerosol pollution and the diurnal changes of heavy rainfall and concurrent clouds in the BTH region and attempted to address the causes. However, although this work has attempted to exclude the impacts from the meteorological background particularly circulation and moisture, the observation study still has its limitation on studying aerosol effect on rainfall and clouds, such as the noise and uncertainty of different observational data, the interaction of aerosol and meteorological factors and the mixing of different types of aerosols. Numerical model simulations are necessarily applied to examine the speculation we proposed here. And the specific processes of aerosol effect on the precipitation formation of mix-phased clouds also needs further exploration in our future study.

Data availability

We are grateful to the National Meteorological Information Centre (NMIC) of the China Meteorological Administration (CMA) for providing hourly precipitation datasets. MODIS aerosol and cloud data were obtained from http://ladsweb.modaps.eosdis.nasa.gov; ultraviolet AI data from OMI was obtained from https://daac.gsfc.nasa.gov/datasets?keywords=OMI&page=1; MACC-II and ERA-interim reanalysis datasets were obtained from http://apps.ecmwf.int/datasets.

Author contributions

JY and SZ conceived the study. SZ processed data and drew the figures. SZ and JY analyzed the observational results and WCW, CZ and DG gave the professional guidance. PS provided the hourly precipitation dataset. SZ and JY prepared the manuscript with contributions from WCW and CZ.

Competing interests

The authors declare that they have no conflict of interest.

Acknowledgements

Jing Yang, Daoyi Gong & Peijun Shi are supported by funds from the National Natural Science Foundation of China (41621061 and 41775071) and the National Key Research and Development Program-Global Change and Mitigation Project: Global Change Risk of Population and Economic System: Mechanism and Assessment (2016YFA0602401), Siyuan Zhou is supported by funds from State Key Laboratory of Earth Surface Processes and Resource Ecology and Key Laboratory of Environmental Change and Natural Disaster. Wei-Chyung Wang acknowledges the support of a grant (to SUNYA) from the Office of Sciences (BER), U.S. DOE. We deeply appreciate two anonymous referees for their indepth comments and constructive suggestions.

References:

Ackerman, A. S.: Reduction of Tropical Cloudiness by Soot, Science, 288(5468), 10421047, doi:10.1126/science.288.5468.1042, 2000.

Albrecht, B. A.: Aerosols, cloud microphysics, and fractional cloudiness, Science, 245(4923), 1227-1230, doi:10.1126/science.245.4923.1227, 1989.

Altaratz, O., Bar-Or, R. Z., Wollner, U., and Koren, I.: Relative humidity and its effect on aerosol optical depth in the vicinity of convective clouds, Environ. Res. Lett., 8, 034025, doi:10.1088/1748-9326/8/3/034025, 2013.

Anonymous: Atmospheric Sciences Thesaurus, China Meteorological Press: Beijing, China, 1994. (in Chinese)

Anonymous: IPCC fifth assessment report, Weather, 68, 310-310, 2013.

615 Bellouin, N., Quaas, J., Morcrette J. -J., and Boucher, O.: Estimates of aerosol radiative forcing from the
616 MACC re-analysis, Atmos. Chem. Phys., 13, 2045-2062, doi:10.5194/acp-13-2045-2013, 2013.
617 Benedetti, A., Morcrette, J. J., Boucher, O., Dethof, A., Engelen, R. J., Fisher, M., Flentje, H., Huneeus, N.,
618 Jones, L., Kaiser, J. W., Kinne, S., Mangold, A., Razinger, M., Simmons, A. J., and Suttie, M.: Aerosol
619 analysis and forecast in the European Centre for Medium-Range Weather Forecasts Integrated Forecast
620 System: 2. Data assimilation, J. Geophys. Res., 114, D13205 doi:10.1029/2008JD011115, 2009.
621 Brennan, J., Kaufman, Y., Koren, I., and Rong, L.: Aerosol-cloud interaction-Misclassification of MODIS
622 clouds in heavy aerosol, IEEE T. Geosci. Remote, 43, 911–915, doi:10.1109/TGRS.2005.844662, 2005.
623 Bennartz, R., and Rausch, J.: Global and regional estimates of warm cloud droplet number concentration
624 based on 13 years of AQUA-MODIS observations, Atmos. Chem. Phys., 17, 9815-9836,
625 doi:10.5194/acp-17-9815-2017, 2017.
626 Bennartz, R.: Global assessment of marine boundary later cloud droplet number concentration from satellite, J.
627 Geophys. Res., 112, D02201, doi:10.1029/2006JD007547, 2007.
628 Boers, R., Acarreta, J. A., and Gras, J. L.: Satellite monitoring of the first indirect aerosol effect: Retrieval of
629 the droplet concentration of water clouds, J. Geophys. Res., 111, D22208, doi:10.1029/2005JD006838,
630 2006.
631 Boucher, O., and Quaas, J.: Water vapour affects both rain and aerosol optical depth, Nat. Geosci., 6(1), 45,
632 doi:10.1038/ngeo1692, 2012.
633 Chen, Q., Yin, Y., Jin, L., Xiao, H., and Zhu, S.: The effect of aerosol layers on convective cloud
634 microphysics and precipitation, Atmos. Res., 101, 327-340, doi:10.1016/j.atmosres.2011.03.007, 2011.
635 Cheng, C. T., Wang, W. C., and Chen, J. P.: A modeling study of aerosol impacts on cloud microphysics and
636 radiative properties, Q. J. R. Meteorol. Soc., 133, 283–297, doi:10.1002/qj.25, 2007.
637 Cheng, C. T., Wang, W. C., and Chen, J. P.: Simulation of the effects of increasing cloud condensation nuclei
638 on mixed-phase clouds and precipitation of a front system, Atmos. Res., 96, 461-476, doi:
639 10.1016/j.atmosres.2010.02.005, 2010.
640 Chylek, P., Dubey, M. K., Lohmann, U., Ramanathan, V., Kaufman, Y. J., Lesins, G., Hudson, J., Altmann,
641 G., and Olsen, S.: Aerosol indirect effect over the Indian Ocean, Geophys. Res. Lett., 33(6), L06806,
642 doi:10.1029/2005GL025397, 2006.
643 Dee, D. P., Uppala, S. M., Simmons, A. J., Berrisford, P., Poli, P., Kobayashi, S., Andrae, U., Balmaseda, M.
644 A., Balsamo, G., Bauer, P., Bechtold, P., Beljaars, A. C. M., van de Berg, L,, Bidlot, J., Bormann, N.,
645 Delsol, C., Dragani, R., Fuentes, M., Geer, A. J., Haimberger, L., Healy, S. B., Hersbach, H., H´olm, E.
646 V., Isaksen, L., K°allberg, P., K¨ohler, M., Matricardi, M., McNally, A. P., Monge-Sanz, B. M.,
647 Morcrette, J. –J., Park, B. –K., Peubey, C., de Rosnay, P., Tavolato, C., Th´epaut, J. –N., Vitart, F.: The
648 ERA-Interim reanalysis: configuration and performance of the data assimilation system, Q. J. R.
649 Meteorol. Soc., 137, 553–597, doi:10.1002/qj.828, 2011.
650 Fan, J. W., Rosenfeld, D., Yang, Y., Zhao, C., Leung, L. R., and Li, Z. Q.: Substantial contribution of

anthropogenic air pollution to catastrophic floods in Southwest China, Geophys. Res. Lett., 42, 6066-6075, doi:10.1002/2015GL064479, 2015.

Garrett, T. J. and Zhao, C.: Increased Arctic cloud longwave emissivity associated with pollution from mid-latitudes, Nature, 440(7085), 787-9, doi:10.1038/nature04636, 2006.

Givati, A., and Rosenfeld, D.: Quantifying precipitation suppression due to air pollution, J. Appl. Meteor., 43, 1038-1056, doi:10.1175/1520-0450(2004)043<1038:QPSDTA>2.0.CO;2, 2004.

Grandey, B. S., and Stier, P.: A critical look at spatial scale choices in satellite-based aerosol indirect effect studies, Atmos. Chem. Phys., 10(23), 11459–11470, doi:10.5194/acp-10-11459-2010, 2010.

Grandey, B. S., Stier, P. and Wagner, T. M.: Investigating relationships between aerosol optical depth and cloud fraction using satellite, aerosol reanalysis and general circulation model data, Atmos. Chem. Phys., 13(6), 31773184, doi:10.5194/acp-13-3177-2013, 2013.

Gryspeerdt, E., Sourdeval, O., Quaas, J., Delanoë, J., Krämer, M., and Kühne, P.: Ice crystal number concentration estimates from lidar–radar satellite remote sensing – Part 2: Controls on the ice crystal number concentration, Atmos. Chem. Phys., 18(19), 14351–14370, doi:10.5194/acp-18-14351-2018, 2018.

Gryspeerdt, E., Stier, P., and Grandey, B. S.: Cloud fraction mediates the aerosol optical depth-cloud top height relationship, Geophys. Res. Lett., 41, 36223627, doi:10.1002/2014GL059524, 2014a.

Gryspeerdt, E., Stier, P., and Partridge, D. G.: Links between satellite-retrieved aerosol and precipitation, Atmos. Chem. Phys., 14, 9677–9694, doi:10.5194/acp-14-9677-2014, 2014b.

Gunthe, S. S., Rose, D., Su, H., Garland, R. M., Achtert, P., Nowak, A., Wiedensohler, A., Kuwata, M., Takegawa, N., Kondo, Y., Hu, M., Shao, M., Zhu, T., Andreae, M. O., and Poschl, U.: Cloud condensation nuclei (CCN) from fresh and aged air pollution in the megacity region of Beijing, Atmos. Chem. Phys., 11(21), 11023-11039, doi:10.5194/acp-11-11023-2011, 2011.

Guo, C. W., Xiao, H., Yang, H. L., and Tang, Q.: Observation and modeling analyses of the macro-and microphysical characteristics of a heavy rain storm in Beijing, Atmos. Res., 156, 125-141, doi:10.1016/j.atmosres.2015.01.007, 2015.

Guo, J. P., Deng, M. J., Lee, S. S., Wang, F., Li, Z. Q., Zhai, P. M., Liu, H., Lv, W., Yao, W., and Li, X. W.: Delaying precipitation and lightning by air pollution over the Pearl River Delta, Part I: Observational analyses. J. Geophys. Res. Atmos., 121, 6472-6488, doi:10.1002/2015JD023257, 2016.

Guo, L., Highwood, E. J., Shaffrey, L. C., and Turner, A. G.: The effect of regional changes in anthropogenic aerosols on rainfall of the East Asian Summer Monsoon, Atmos. Chem. Phys., 13, 1521-1534, doi:10.5194/acp-13-1521-2013, 2013.

Guo, X. L., Fu, D. H., Guo, X., and Zhang, C. M.: A case study of aerosol impacts on summer convective clouds and precipitation over northern China, Atmos. Res., 142, 142-157, doi:10.1016/j.atmosres.2013.10.006, 2014.

Hammer, M. S., Martin, R. V., Li, C., Torres, O., Manning, M., and Boys, B. L.: Insight into global trends in

687 aerosol composition from 2005 to 2015 inferred from the OMI Ultraviolet Aerosol Index, Atmos. Chem.
688 Phys., 18, 8097-8112, doi:10.5194/acp-18-8097-2018, 2018.
689 Harikishan, G., Padmakumari, B., Maheskumar, R. S., Pandithurai, G., and Min, Q. L.: Aerosol indirect effects
690 from ground-based retrievals over the rain shadow region in Indian subcontinent, J. Geophys. Res.
691 Atmos., 121(5), 2369-2382, doi:10.1002/2015JD024577, 2016.
692 Higgins, R. W., Yao, Y., Yarosh, E. S., Janowiak, J. E. and Mo, K. C.: Influence of the Great Plains low-level
693 jet on summertime precipitation and moisture transport over the central United States, J. Climate, 10,
694 481-507, doi:10.1175/1520-0442(1997)010<0481:IOTGPL>2.0.CO;2, 1997.
695 Holz, R. E., Ackerman, S. A., Nagle, F. W., Frey, R., Dutcher, S., Kuehn, R. E., Vaughan, M. A., and Baum,
696 B.: Global Moderate Resolution Imaging Spectroradiometer (MODIS) cloud detection and height
697 evaluation using CALIOP, J. Geophys. Res. Atmos., 113, D00A19, doi: 10.1029/2008JD009837, 2008.
698 Jacobson, M. Z.: Strong radiative heating due to the mixing state of black carbon in atmospheric aerosols,
699 Nature, 409, 695-697, doi:10.1038/35055518, 2001.
700 Jiang, H., Feingold, G., and Cotton, W. R.: Simulations of aerosol-cloud-dynamical feedbacks resulting from
701 entrainment of aerosol into the marine boundary layer during the Atlantic Stratocumulus Transition
702 Experiment, J. Geophys. Res., 107(D24), 4813, doi:10.1029/2001JD001502, 2002.
703 Jiang, J. H., Su, H., Schoeberl, M. R., Massie, S. T., Colarco, P., Platnick, S., and Livesey, N. J.: Clean and
704 polluted clouds: Relationships among pollution, ice clouds, and precipitation in South America, Geophys.
705 Res. Lett., 35, L14804, doi: 10.1029/2008GL034631, 2008.
706 Jiang, M. J., Li, Z. Q., Wan, B. C., and Cribb, M.: Impact of aerosols on precipitation from deep convective
707 clouds in eastern China, J. Geophys. Res., 121, 9607-9620, doi:10.1002/2015JD024246, 2016.
708 Johnson, D. B.: The role of giant and ultra-giant aerosol particles in warm rain initiation, J. Atmos. Sci., 39,
709 448–460, doi:10.1175/1520-0469(1982)039<0448:TROGAU>2.0.CO;2, 1982.
710 Jung, W. S., Panicker, A. S., Lee, D. I., and Park, S. H.: Estimates of aerosol indirect effect from Terra
711 MODIS over Republic of Korea, Advances in Meteorology, 2013 (976813), 1-8,
712 doi:10.1155/2013/976813, 2013.
713 Kim, K. –M., Lau, K. M., Sud, Y. C., and Walker, G. K.: Influence of aerosol radiative forcings on the diurnal
714 and seasonal cycles of rainfall over West Africa and Eastern Atlantic Ocean using GCM simulation, Clim.
715 Dyn., 35(1), 115-126, doi: 10.1007/s00382-010-0750-1, 2010.
716 Lau, K. M., Kim, M. K., and Kim, K. M.: Asian summer monsoon anomalies induced by aerosol direct
717 forcing: the role of the Tibetan Plateau, Clim. Dyn., 26, 855-864, doi:10.1007/s00382-006-0114-z, 2006.
718 Lee, S. S., Donner, L. J., and Phillips, V. T. J.: Impacts of aerosol chemical composition on microphysics and
719 precipitation in deep convection, Atmos. Res., 94, 220-237, doi:10.1016/j.atmosres.2009.05.015, 2009.
720 Lee, S. S., Guo, J., and Li, Z: Delaying precipitation by air pollution over the Pearl River Delta: 2. Model
721 simulation, J. Geophys. Res. Atmos., 121, 11739-11760, doi:10.1002/2015JD024362, 2016.
722 Lelieveld, J. and Heintzenberg, J.: Sulfate cooling effect on climate through in-cloud oxidation of

723 anthropogenic SO2, Science, 258, 117-120, doi:10.1126/science.258.5079.117, 1992.
724 Levy, R. C., Mattoo, S., Munchak, L. A., Remer, L. A., Sayer, A. M., Patadia, F., and Hsu, N. C.: The
725 Collection 6 MODIS aerosol products over land and ocean, Atmos. Meas. Tech., 6, 2989–3034,
726 doi:10.5194/amt-6-2989-2013, 2013.
727 Li, H., Cui, X., Zhang, W., and Qiao, L.: Observational and dynamic downscaling analysis of a heavy rainfall
728 event in Beijing, China during the 2008 Olympic Games, Atmos. Sci. Lett., 17, 368-376,
729 doi:10.1002/asl.667, 2016.
730 Li, Z., Niu, F., Fan, J., Liu, Y., Rosenfeld, D., and Ding, Y.: Long-term impacts of aerosols on the vertical
731 development of clouds and precipitation, Nat. Geosci., 4, 888-894, doi:10.1038/ngeo1313, 2011.
732 Lim, K. S. and Hong, S.: Investigation of aerosol indirect effects on simulated flash-flood heavy rainfall over
733 Korea, Meteor. Atmos. Phys., 118, 199-214, doi:10.1007/s00703-012-0216-6, 2012.
734 Liu, G., Shao, H., Coakley Jr. J. A., Curry, J. A., Haggerty, J. A., and Tschudi, M. A.: Retrieval of cloud
735 droplet size from visible and microwave radiometric measurements during INDOEX: Implication to
736 aerosols' indirect radioactive effect, J. Geophys. Res., 108(D1), 4006, doi:10.1029/2001JD001395, 2003.
737 Liu, J., Wang, S., Zhang, W., and Wei, X.: Mechanism analysis of a strong convective weather in Hebei
738 Province, Advances in Marine Science, 30, 9-16, 2012. (in Chinese)
739 Menzel, W. P., Frey, R. A., Zhang, H., Wylie, D. P., Moeller, C. C., Holz, R. E., Maddux, B., Baum, B. A.,
740 Strabala, K. I., and Gumley, L. E.: MODIS global cloud-top pressure and amount estimation: Algorithm
741 description and results, J. Appl. Meteorol. Clim., 47(4), 1175-1198, doi: 10.1175/2007JAMC1705.1,
742 2008.
743 Min, Q., Joseph, E., Lin, Y., Min, L., Yin, B., Daum, P. H., Kleinman, L. I., Wang, J., and Lee, Y. –N.:
744 Comparison of MODIS cloud microphysical properties with in-situ measurements over the Southeast
745 Pacific, Atmos. Chem. Phys., 12, 11261-11273, doi:10.5194/acp-12-11261-2012, 2012.
746 Nakajima, T. and King, M. D.: Determination of the optical thickness and effective particle radius of clouds
747 from reflected solar radiation measurements. Part I: Theory, J. Atmos. Sci., 47, 1878-1893,
748 doi:10.1175/1520-0469(1990)047<1878:DOTOTA>2.0.CO;2, 1990.
749 Panicker, A. S., Pandithurai, G., and Dipu, S.: Aerosol indirect effect during successive contrasting monsoon
750 seasons over Indian subcontinent using MODIS data, Atmos. Environ., 44(15), 1937-1943,
751 doi:10.1016/j.atmosenv.2010.02.015, 2010.
752 Platnick, S., Meyer, K., King, M. D., Wind, G., Amarasinghe, N., Marchant, B., Arnold, G. T., Zhang, Z.,
753 Hubanks, P. A., Holz, R. E., Yang, P., Ridgway, W. L., and Riedi, J.: The MODIS cloud optical and
754 microphysical products: Collection 6 updates and examples from Terra and Aqua, IEEE Trans. Geosci.
755 Remote Sens., 55, 502-525, doi:10.1109/TGRS.2016.2610522, 2017.
756 Qian, Y., Gong, D. Y., Fan, J. W., Leung, L. R., Bennartz, R., Chen, D. L., Wang, W. G.: Heavy pollution
757 suppresses light rain in China: Observations and modeling, J. Geophys. Res. Atmos., 114, D00K02,
758 doi:10.1029/2008JD011575, 2009.

Qiu, Y., Zhao, C., Guo, J., and Li, J.: 8-Year ground-based observational analysis about the seasonal variation of the aerosol-cloud droplet effective radius relationship at SGP site, Atmos. Environ., 164, 139-146, doi:10.1016/j.atmosenv.2017.06.002, 2017.

Quaas, J., Boucher, O., Bellouin, N. and Kinne, S.: Satellite-based estimate of the direct and indirect aerosol climate forcing, J. Geophys. Res., 113, D05204, doi:10.1029/2007JD008962, 2008.

Quaas, J., Stevens, B., Stier, P., and Lohmann U.: Interpreting the cloud cover aerosol optical depth relationship found in satellite data using a general circulation model, Atmos. Chem. Phys., 10(13), 61296135, doi:10.5194/acp-10-6129-2010, 2010.

Rienecker, M. M., Suarez, M. J., Todling, R., Bacmeister, J., Takacs, L., Liu, H. C., Gu, W., Sienkiewicz, M., Koster, R. D., Gelaro, R., Stajner, I., Nielsen, J. E.: The GEOS-5 Data Assimilation System—Documentation of Versions 5.0.1 and 5.1.0, and 5.2.0. NASA Technical Report Series on Global Modeling and Data Assimilation NASA/TM-2008 -104606 27: 92 pp, 2008.

Rosenfeld, D.: TRMM observed first direct evidence of smoke from forest fires inhibiting rainfall, Geophys. Res. Lett., 26, 3105–3108, doi:10.1029/1999GL006066, 1999.

Rosenfeld, D., Lohmann, U., Raga, G. B., O'Dowd, C. D., Kulmala, M., Fuzzi, S., Reissell, A., Andreae, M. O.: Flood or drought: How do aerosols affect precipitation? Science, 321, 1309-1313, doi:10.1126/science.1160606, 2008.

Rosenfeld, D., Sherwood, S., Wood, R., and Donner, L.: Climate effects of aerosol-cloud interactions, Science, 343, 379-380, doi:10.1126/science.1247490, 2014.

Rosenfeld, D., and Woodley, W. L.: Convective clouds with sustained highly supercooled liquid water down to -37.5°C, Nature, 405, 440–442, doi:10.1038/35013030, 2000.

Sassen, K., Starr, D., Mace, G. G., Poellot, M. R., Melfi, S. H., Eberhard, W.L., Spinhirne, J. D., Eloranta, E. W., Hagan, D. E., and Hallett, J.: The 5–6 December 1991 FIRE IFO II jet stream cirrus case study: Possible influences of volcanic aerosols, J. Atmos. Sci., 52, 97–123, doi:10.1175/1520-0469(1995)052<0097:TDFIIJ>2.0.CO;2, 1995.

Shen, Y., Xiong, A., Wang, Y., and Xie, P.: Performance of high-resolution satellite precipitation products over China, J. Geophys. Res., 115, D02114, doi:10.1029/2009JD012097, 2010.

Sherwood, S.: Aerosols and ice particle size in tropical cumulonimbus, J. Clim., 15, 1051–1063, doi:10.1175/1520-0442(2002)015<1051:AAIPSI>2.0.CO;2, 2002.

Shinozuka, Y., Clarke, A. D., Nenes, A., Jefferson, A., Wood, R., McNaughton, C. S., Ström, J., Tunved, P., Redemann, J., Thornhill, K. L., Moore, R. H., Lathem, T. L., Lin, J. J., and Yoon, Y. J.: The relationship between cloud condensation nuclei (CCN) concentration and light extinction of dried particles: indications of underlying aerosol processes and implications for satellite-based CCN estimates, Atmos. Chem. Phys., 15, 7585-7604, doi:10.5194/acp-15-7585-2015, 2015.

Song, X. L. and Zhang, G. J.: Microphysics parameterization for connective clouds in a global climate model: Description and single-column model tests, J. Geophys. Res. Atmos., 116, D02201,

795 doi:10.1029/2010JD014833, 2011.
796 Squires, P.: The growth of cloud drops by condensation: I. general characteristics, Aust. J. Sci. Res., Ser. A, 5,
797 66–86, 1952.
798 Squires, P., and Twomey, S.: A comparison of cloud nucleus measurements over central North America and
799 Caribbean Sea, J. Atmos. Sci., 23, 401–404, doi: 10.1175/1520-0469(1966)023<0401:ACOCNM>
800 -2.0.CO;2, 1966.
801 Sun, Y. L., Wang, Z. F., Du, W., Zhang, Q., Wang, Q. Q., Fu, P. Q., Pan, X. L., Li, J., Jayne, J., and Worsnop,
802 D. R.: Long-term real-time measurements of aerosol particle composition in Beijing, China: seasonal
803 variations, meteorological effects, and source analysis, Atmos. Chem. Phys., 15, 10149-10165,
804 doi:10.5194/acp-15-10149-2015, 2015.
805 Tariq, S., and Ali, M.: Spatio-temporal distribution of absorbing aerosols over Pakistan retrieved form OMI on
806 board Aura Satellite, Atmos. Pollution Res., doi: 10.5094/APR.2015.030, 2015.
807 Tao, M. H., Chen, L. F., Wang, Z. F., Tao, J. H., Che, H. Z., Wang, X. H., and Wang, Y.: Comparison and
808 evaluation of the MODIS Collection 6 aerosol data in China, J. Geophys. Res. Atmos., 120, 6992-7005,
809 doi:10.1002/2015JD023360, 2015.
810 Tao, W. K., Chen, J. P., Li, Z., Wang, C., and Zhang C.: Impact of aerosols on convective clouds and
811 precipitation, Rev. Geophy., 50, RG2001/2012, 1-62, doi: 10.1029/2011RG000369, 2012.
812 Torres, O., Bhartia, P.K., Herman, J.R., Ahmad, Z., Gleason, J.: Derivation of aerosol properties from satellite
813 measurements of backscattered ultraviolet radiation: Theoretical basis, J. Geophys. Res. Atmos., 103,
814 17099–17110, doi:10.1029/98JD00900, 1998.
815 Twohy, C. H., Coakley, J. A., and Tahnk, W. R.: Effect of changes in relative humidity on aerosol scattering
816 near clouds, J. Geophys. Res. Atmos., 114, D05205, doi:10.1029/2008JD010991, 2009.
817 Twomey, S.: The influence of pollution on the shortwave albedo of clouds, J. Atmos. Sci., 34, 1149–1152,
818 doi:10.1175/1520-0469(1977)034<1149:TIOPOT>2.0.CO;2, 1977.
819 Wang, J., Feng, J., Wu, Q., and Z. Yan, Z.: Impact of anthropogenic aerosols on summer precipitation in the
820 Beijing-Tianjin-Hebei urban agglomeration in China: Regional climate modeling using WRF-Chem, Adv.
821 Atmos. Sci., 33, 753-766, doi:10.1007/s00376-015-5103-x, 2016.
822 Wolyn, P. G., and Mckee, T. B.: The mountain plains circulation east of a 2-km-high north south barrier, Mon.
823 Weather Rev., 122, 1490-1508, doi:10.1175/1520-0493(1994)122<1490:TMPCEO>2.0.CO;2, 1994.
824 Wu, P., Ding, Y. H., and Liu, Y. J.: Atmospheric circulation and dynamic mechanism for persistent haze
825 events in the Beijing-Tianjin-Hebei region, Adv. Atmos. Sci., 34(4), 429-440,
826 doi:10.1007/s00376-016-6158-z, 2017.
827 Yang, X., Zhao, C., Zhou, L., Li, Z., Cribb, M., and Yang, S.: Wintertime cooling and a potential connection
828 with transported aerosols in Hong Kong during recent decades, Atmos. Res., 211, 52-61,
829 doi:10.1016/j.atmosres.2018.04.029, 2018.
830 Yu, R. C., Zhou, T. J., Xiong, A. Y., Zhu, Y. J., and Li, J. M.: Diurnal variations of summer precipitation over

contiguous China, Geophys. Res. Lett, 34, L017041, doi:10.1029/2006GL028129, 2007.

Yuan, T., Li, Z., Zhang, R., and Fan, J.: Increase of cloud droplet size with aerosol optical depth: An observation and modeling study, J. Geophys. Res. Atmos., 113, D04201, doi:10.1029/2007JD008632, 2008.

Yuan, W. H., Yu, R. C., Chen, H. M., Li, J., and Zhang, M. H.: Subseasonal Characteristics of Diurnal Variation in Summer Monsoon Rainfall over Central Eastern China, J. Climate, 23,6684-6695, doi:10.1175/2010JCLI3805.1, 2010.

Zeng, S., Riedi, J., Trepte, C. R., Winker, D. M., and Hu, Y. –X.: Study of global cloud droplet number concentration with A-Train satellites, Atmos. Chem. Phys., 14, 7125-7134, doi: 10.5194/acp-14-7125-2014, 2014.

Zhao, B., Gu, Y., Liou, K. -N., Wang, Y., Liu, X., Huang, L., Jiang, J. H., and Su, H.: Type-Dependent Responses of Ice Cloud Properties to Aerosols From Satellite Retrievals, Geophys. Res. Lett., 45(7), 3297–3306, doi:10.1002/2018GL077261, 2018.

Zhou, S., Yang, J., Wang, W. C., Gong, D., Shi, P., and Gao, M.: Shift of daily rainfall peaks over the Beijing–Tianjin–Hebei region: An indication of pollutant effects? Int. J. Climatol. 2018;1–10, doi:10.1002/joc.5700, 2018.

Zhu, Y., Rosenfeld, D., and Li, Z.: Under what conditions can we trust retrieved cloud drop concentrations in broken marine stratocumulus? J. Geophys. Res. Atmos., 123, 8754-8767, doi:10.1029/2017JD028083, 2018.

Tables

Indicator	Source	Begin time	Thresholds	
			25th percentile	75th percentile
AOD	MODIS	2002	0.98	2.00
CDNC (cm^{-3})	MODIS	2002	30.10	91.03
AAI	OMI	2005	0.13	0.52
SAI	OMI	2005	- 0.13	- 0.35
AOD of BC	MACC	2003	0.04	0.06
AOD of sulfate	MACC	2003	0.46	0.87
SH at 850 hPa (g/kg)	ERA-interim	2002	9.96	12.95

Table 1. The indicators and their sources, begin times and the thresholds used in the study. The end time of all data is to 2012.

Characteristics of heavy rainfall	Clean		Polluted		Difference		Significance	
	AOD	CDNC	AOD	CDNC	AOD	CDNC	AOD	CDNC
Start time	24.2 (3.9)	24.3 (4.0)	23.5 (4.8)	22.9 (3.9)	- 0.7	- 1.4	P<0.05	P<0.05
Peak time	23.0 (4.0)	22.1 (5.3)	22.0 (4.8)	19.1 (5.7)	- 1.0	- 3.0	P<0.05	P<0.05
Duration	4.0 (2.1)	5.5 (3.3)	4.8 (2.8)	7.7 (4.3)	0.8	2.2	P<0.05	P<0.05
Intensity	164.9 (98.4)	166.0 (89.3)	169.6 (94.3)	162.7 (89.1)	4.7	- 3.3	P>0.1	P>0.1

Table 2. The mean values of start time (units: LST), peak time (units: LST), duration (units: hours) and intensity (units: 0.1mm/hour) of heavy rainfall respectively on the clean and polluted conditions using two indicators of AOD and CDNC, and their differences (polluted minus clean) and significances. The numbers in the brackets stand for the standard deviations on the means. "P<0.05" stands for the difference has passed the significance test of 95%, and "P>0.1" stands for the difference did not pass the significance test of 90%.

Characteristics of heavy rainfall	AAI	SAI	Difference (AAI-SAI)	Less BC	More BC	Difference (More-Less)	Less sulfate	More sulfate	Difference (More-Less)
Start time	23.4 (4.8)	24.1 (4.4)	-0.7	24.2 (4.8)	23.9 (4.4)	-0.3	24.0 (4.3)	24.5 (4.4)	0.5
Peak time	21.0 (5.3)	22.6 (5.1)	-1.6	23.4 (5.3)	22.3 (4.0)	-1.1	23.2 (4.5)	22.9 (4.8)	-0.3
Duration	5.0 (3.1)	6.0 (3.8)	-1.0	4.8 (2.6)	4.6 (2.7)	-0.2	4.0 (2.1)	5.5 (3.0)	1.5

Table 3. The mean values of start time (units: LST), peak time (units: LST) and duration (units: hours) of heavy rainfall respectively on the conditions with more absorbing aerosols (AAI more than 75th percentile), more scattering aerosols (SAI more than 75th percentile), less or more BC (AOD of BC less than 25th or more than 75th percentile), less or more sulfate (AOD of sulfate less than 25th or more than 75th percentile), and their differences. Numbers in the brackets stand for the standard deviations on the means. All differences have passed the significant test of 95%.

Clean/Polluted		CF	CTP	COT		CWP		CER	
				liquid	ice	liquid	ice	liquid	ice
AOD	Clean	62.8 (17.6)	442.3 (149.6)	6.9 (4.5)	6.7 (8.5)	62.8 (36.6)	123.1 (168.9)	16.7 (4.4)	32.0 (8.7)
	Polluted	89.3 (12.9)	487.3 (145.7)	10.0 (5.8)	12.9 (17.0)	96.4 (52.5)	211.3 (279.3)	17.5 (3.5)	29.2 (9.0)
CDNC	Clean	94.5 (6.1)	398.0 (131.7)	8.1 (6.0)	8.7 (10.6)	102.4 (104.3)	171.6 (204.3)	20.4 (2.8)	34.2 (6.0)
	Polluted	97.4 (4.2)	430.8 (135.2)	40.4 (21.5)	33.1 (22.7)	318.2 (213.2)	542.5 (447.8)	12.2 (1.9)	25.4 (8.7)

Table 4. The mean values of CF (units: %), CTP (units: hPa), COT (liquid and ice, units: none), CWP (liquid and ice, units: g/m^2) and CER (liquid and ice, units: μm) on the clean condition (less than 25th percentile) and polluted condition (more than 75th percentile) using two indicators of AOD and CDNC. Numbers in the brackets stand for the standard deviations on the means. The differences between clean and polluted conditions have all passed the significant test of 95%.

Group (case number)		CF	CTP	COT		CWP		CER	
				liquid	ice	liquid	ice	liquid	ice
1	Clean, dry (153)	93.8 (6.1)	393.3 (117.3)	7.2 (4.6)	7.6 (9.4)	88.7 (70.6)	149.0 (146.4)	20.4 (3.0)	36.7 (6.6)
2	Polluted, dry (128)	95.6 (5.1)	475.7 (142.8)	50.2 (24.4)	43.4 (19.3)	424.6 (275.5)	793.5 (404.7)	12.6 (2.4)	30.0 (7.0)
3	Clean, wet (155)	*92.7 (7.0)* $p_{1,3}>0.05$	457.4 (191.0)	8.6 (4.7)	10.6 (12.6)	101.9 (64.5)	207.7 (254.1)	*19.8 (2.5)* $p_{1,3}>0.05$	33.2 (4.4)
4	Polluted, wet (194)	97.8 (4.4)	*419.7 (141.0)* $p_{3,4}>0.05$	36.4 (20.6)	28.4 (21.1)	295.9 (208.7)	456.4 (412.1)	*12.5 (2.0)* $p_{2,4}>0.1$	24.4 (7.5)

Table 5. The mean values of CF (units: %), CTP (units: hPa), COT (liquid and ice, units: none), CWP (liquid and ice, units: g/m^2) and CER (liquid and ice, units: μm) in four groups. Numbers in the brackets stand for the standard deviations on the means. Italic numbers in grey represent that the differences are not significant, in which "P>0.05" stands for the difference has passed the significance test of 90% but did not pass the significance test of 95%, and "P>0.1" stands for the difference did not pass the significance test of 90%.

Figures

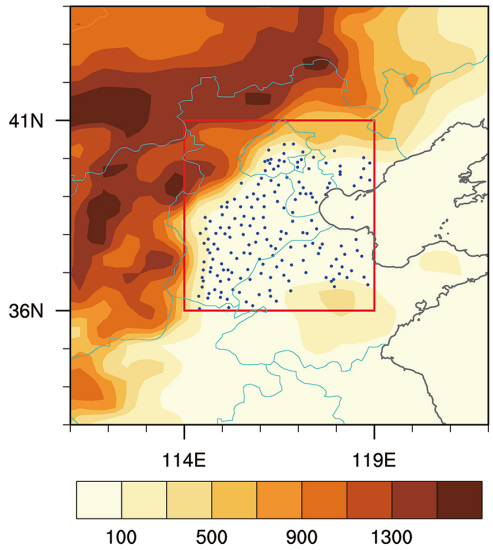

Figure 1. Altitudes (shading, units: m) and selected stations (dots) in the BTH region (red box, 36–41° N, 114–119° E).

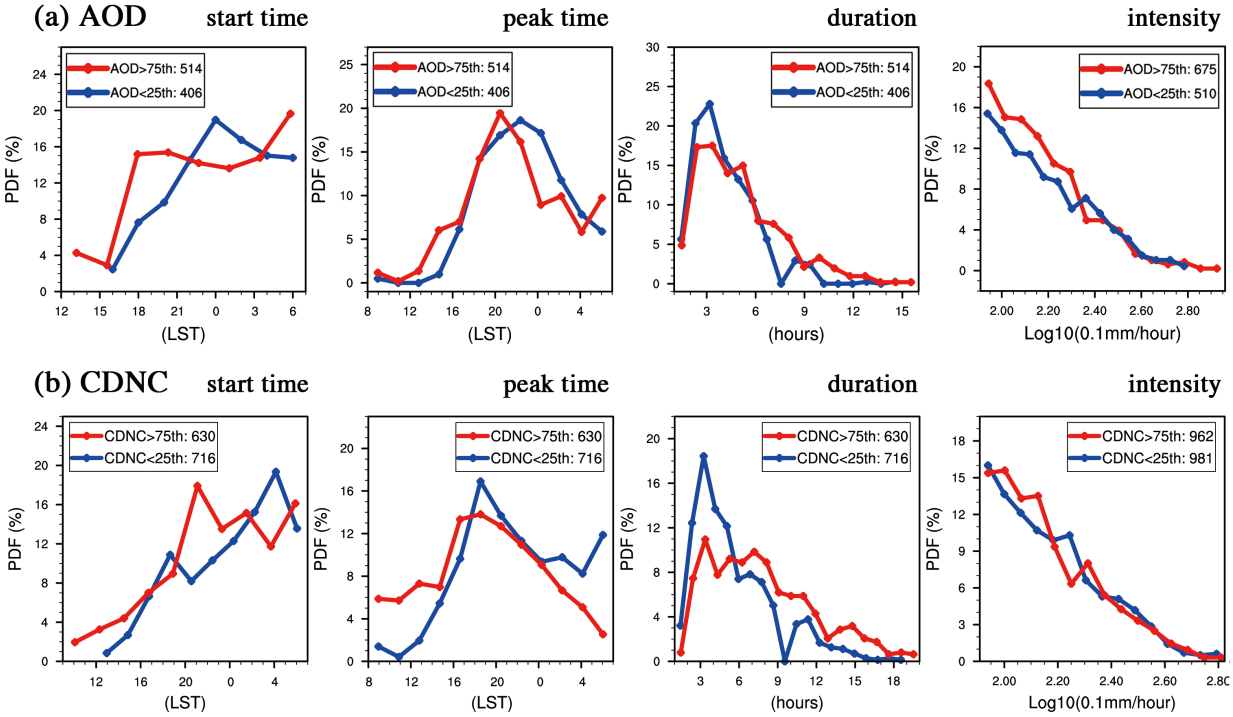

Figure 2. PDF of start time (units: LST), peak time (units: LST), duration (units: hours) and intensity (units: 0.1mm/hour) of heavy rainfall on selected clean (blue lines) and polluted (red lines) conditions, respectively using indicator of (a) AOD and (b) CDNC (cm^{-3}), during early summers from 2002 to 2012.

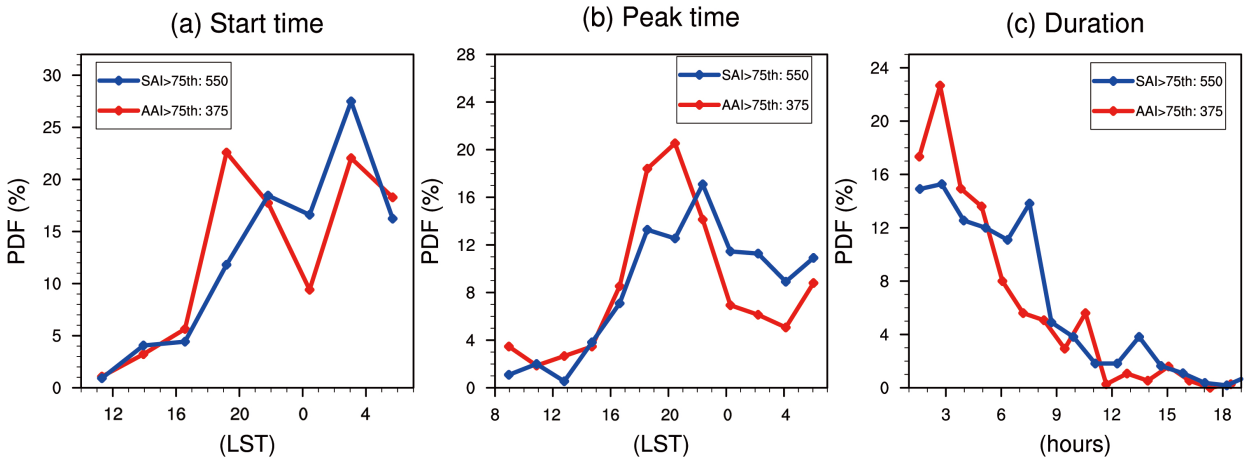

Figure 3. PDF of (a) start time (units: LST), (b) peak time (units: LST), and (c) duration (units: hours) of heavy rainfall on the days with SAI more than 75th percentile (blue lines) and days with AAI more than 75th percentile (red lines), during early summers from 2005 to 2012.

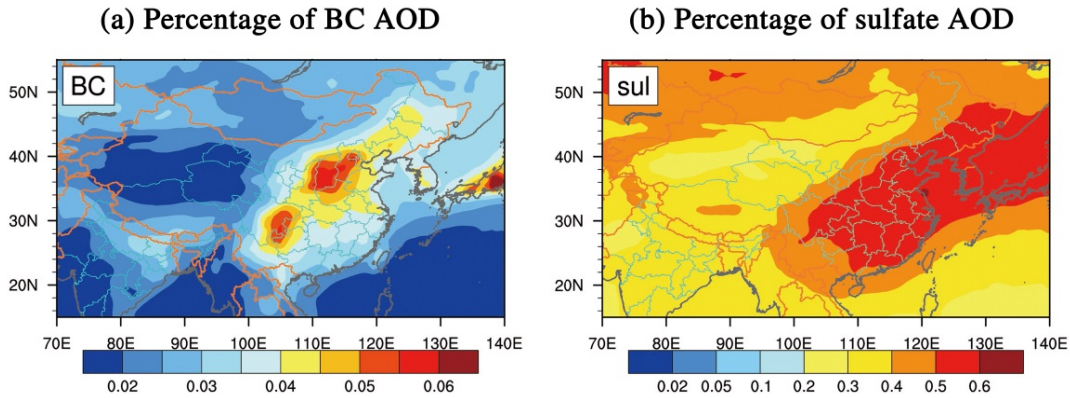

Figure 4. Percentages of AOD for (a) BC and (b) sulfate in JJA during 2002 to 2012.

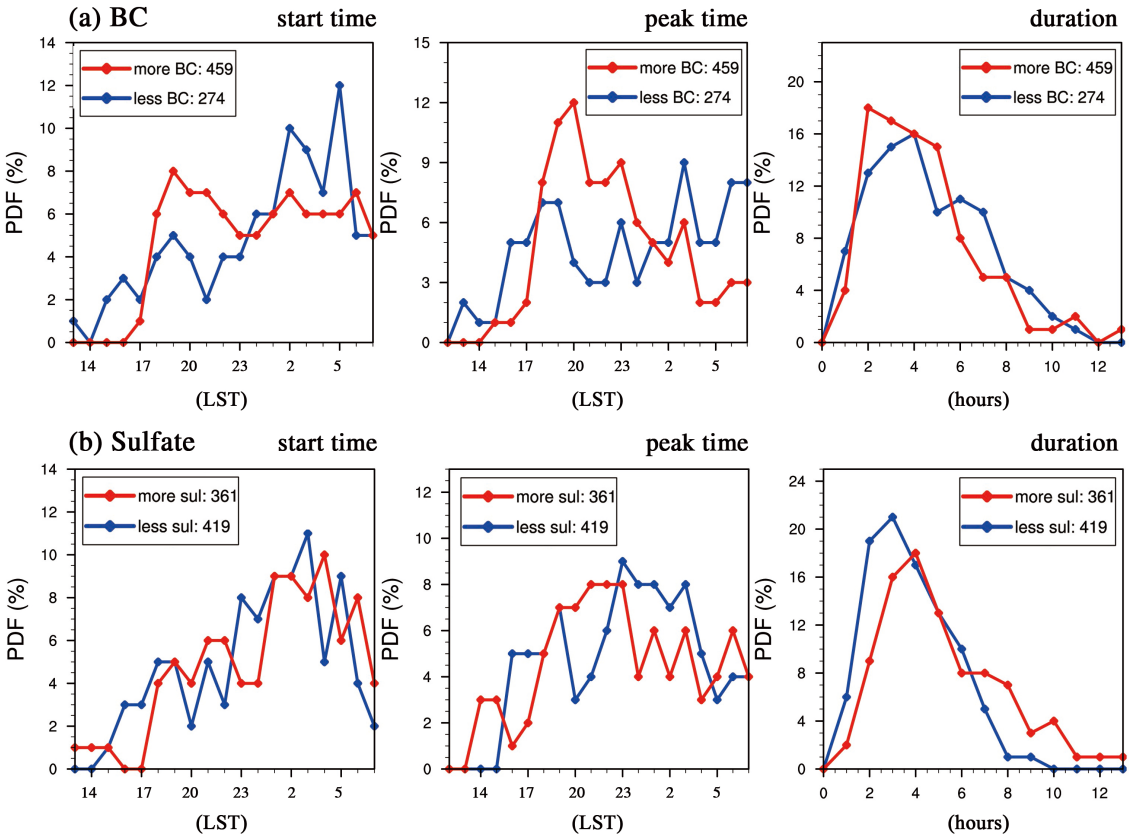

Figure 5. PDF of start time (units: LST), peak time (units: LST) and duration (units: hours) of heavy rainfall in different conditions of (a) BC and (b) sulfate. Blue/red lines stand for the condition of less/more BC or sulfate (AOD of BC or sulfate less than 25th /more than 75th percentile) during early summers from 2003 to 2012.

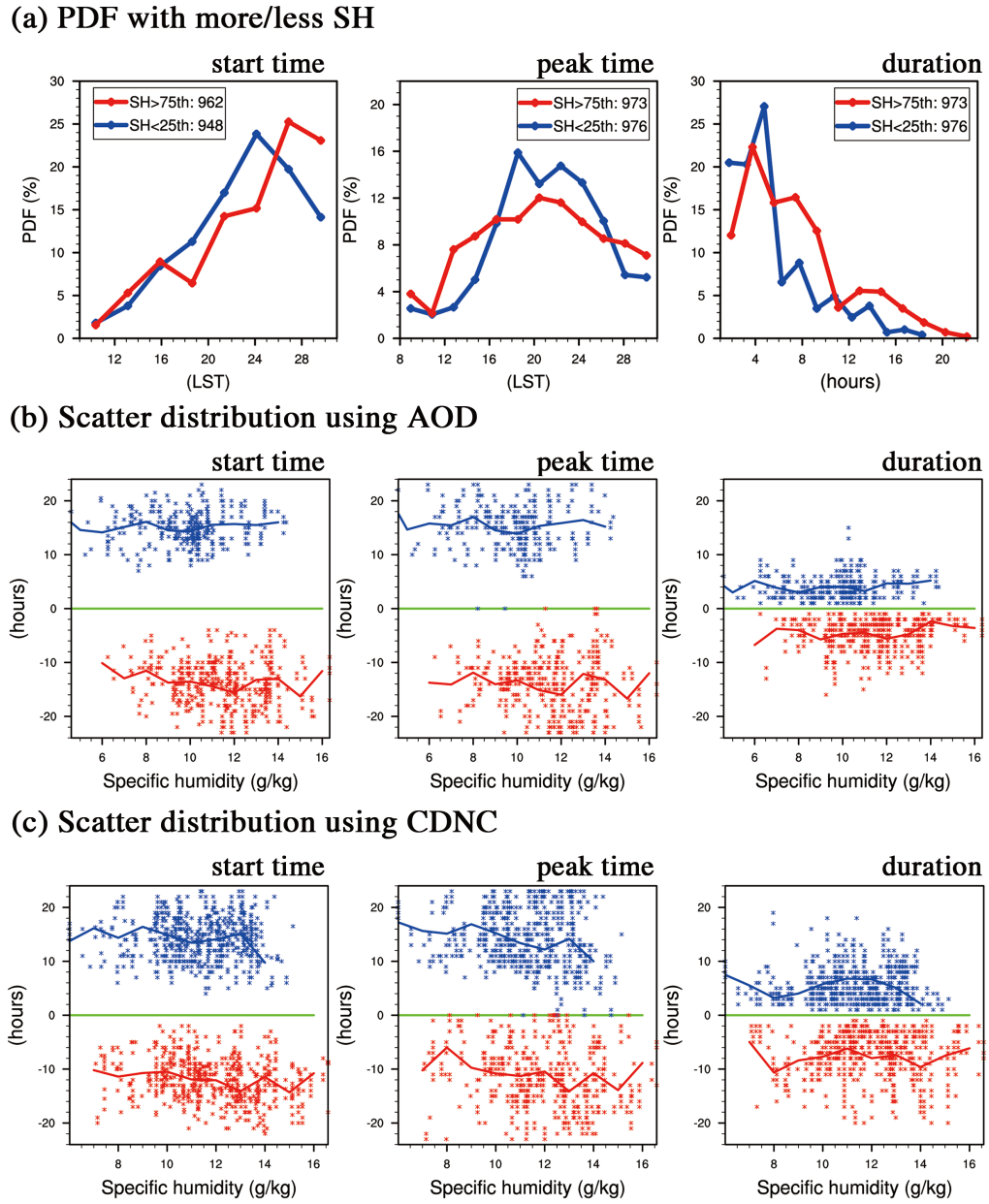

Figure 6. (a) PDF of start time (units: LST), peak time (units: LST), and duration (units: hours) of heavy rainfall with less moisture (blue lines, SH at 850 hPa less than 25th percentile) and more moisture (red lines, SH at 850 hPa more than 75th percentile). (b) and (c) are scatter distributions of SH-start time/peak time/duration for clean cases (blue points) and polluted cases (red points) respectively using AOD and CDNC. Green lines stands for the start/peak time at 8:00 LST or duration is 0 hours. Positive (negative) values stand for the hours away from 8:00 LST or 0 hours in clean (polluted) cases. Blue (red) lines stand for the mean values of rainfall characteristics at each integer of SH in clean (polluted) cases.

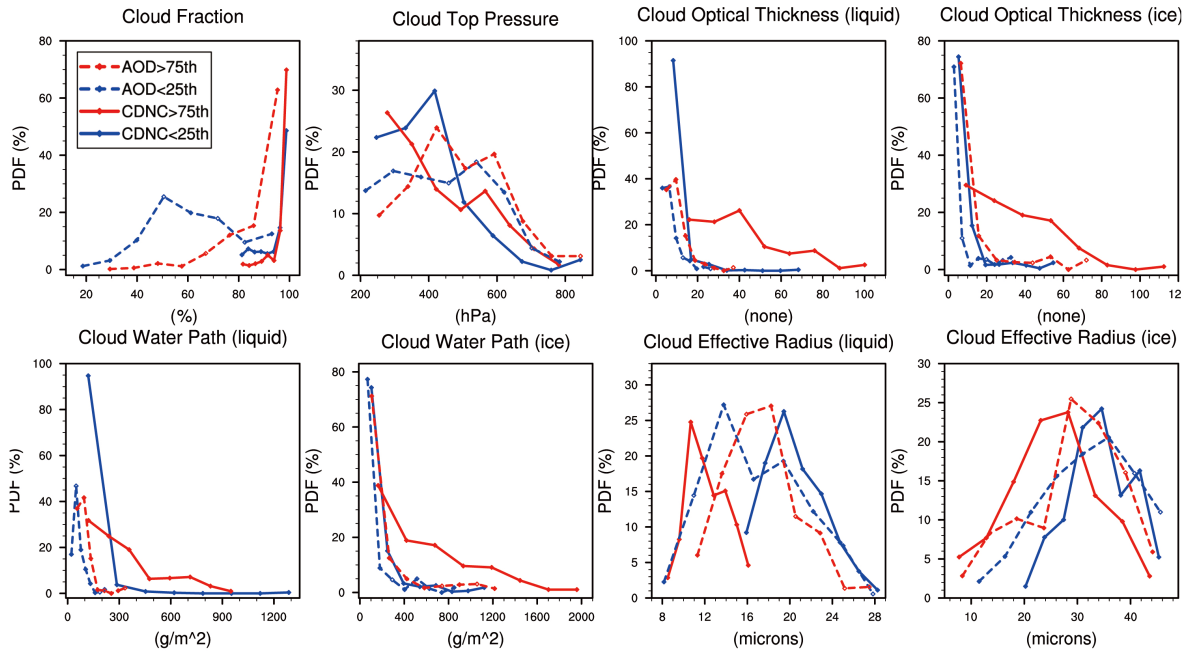

977

978 Figure 7. PDF of CF (units: %), CTP (units: hPa), COT (liquid and ice, units: none), CWP (liquid and ice,
979 units: g/m^2) and CER (liquid and ice, units: μm) on selected clean (blue dash lines: AOD<25th percentile; blue
980 solid lines: CDNC<25th percentile) and polluted (red dash lines: AOD>75th percentile; red solid lines:
981 CDNC>75th percentile) heavy rainfall days.

982

983

984

985

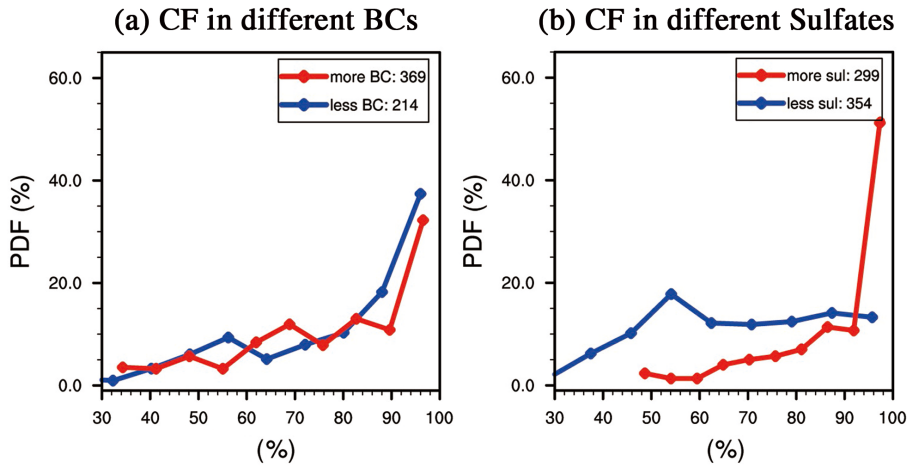

986

987 Figure 8. PDF of CF (units: %) respectively for the conditions of less BC/sulfate (blue lines, AOD of
988 BC/sulfate less than 25th percentile) and more BC/sulfate (red lines, AOD of BC/sulfate more than 75th
989 percentile) cases with heavy rainfall during 10 early summers (2003-2012).

990

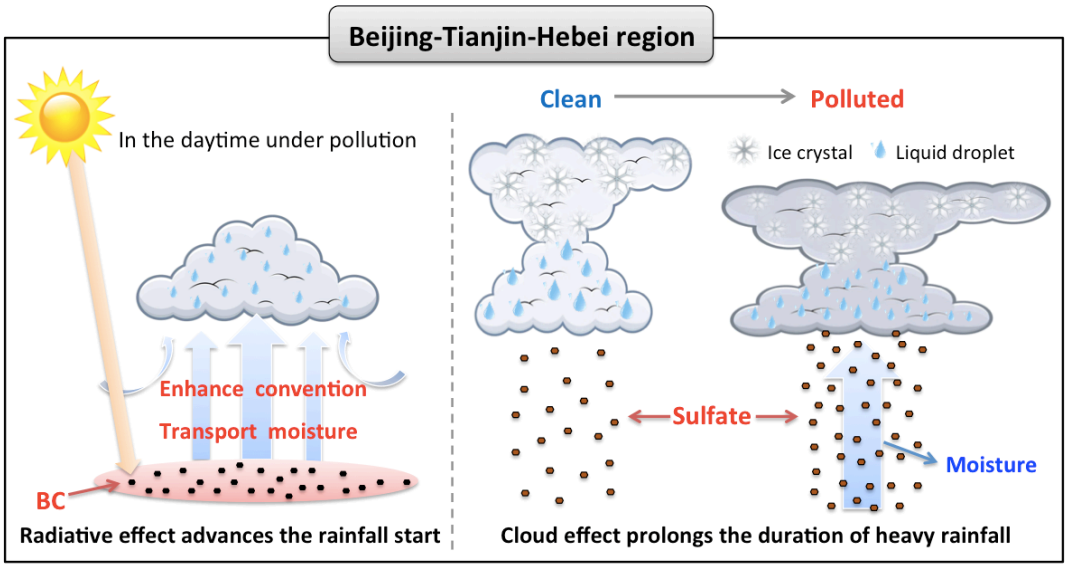

Figure 9. A schematic diagram for aerosol impacts on heavy rainfall over Beijing-Tianjin-Hebei region.